J. Materials, Conc. Struct., Pavements, JSCE, No.655/V-48, 143-157, 2000 August

NUMERICAL SIMULATION ON CORROSION OF STEEL IN CONCRETE STRUCTURES UNDER CHLORIDE ATTACK

Kai-Lin HSU[1], Hitoshi TAKEDA[2] and Tsuyoshi MARUYA[3]

[1]Member of JSCE, Ph.D., Researcher, Technology Research Center, Taisei Corporation (344-1 Nase-cho, Totsuka-ku, Yokohama 245-0051, Japan)

[2]Member of JSCE, Researcher, Technology Research Center, Taisei Corporation (344-1 Nase-cho, Totsuka-ku, Yokohama 245-0051, Japan)

[3]Member of JSCE, Dr.Eng., Researcher, Technology Research Center, Taisei Corporation (344-1 Nase-cho, Totsuka-ku, Yokohama 245-0051, Japan)

One comprehensive numerical system is proposed for the attempt to solve the problem related to deterioration of reinforced concrete (RC) structures under chloride-induced corrosion. This numerical system is characterized by combining the physico-chemical models related to the migration of corrosion-related substances in concrete, such as chloride, oxygen and moisture, and the electrochemical models dealing with the formation of natural potential and corrosion current of RC members under chloride-induced corrosion. Experimental comparison indicated the availability of this numerical system on modeling corrosion of steel in concrete structures under chloride attack.

Key Words: *mass migration, macrocell corrosion, durability, concrete deterioration, chloride attack*

1. INTRODUCTION

By adopting the proposal of Miyagawa[1] *et al.*, the process of the deterioration and degradation of concrete structures exposed to corrosive environment can be generally classified as four stages: incubation period, propagation period, and acceleration period and deterioration period. As indicated in the review article of Takewaka[2] *et al.*, for those research works related to the above classification, the following observations were implied. First, the models on describing the deterioration process in incubation period are believed to be quantitatively reliable. Secondly, according to the distribution of corrosion-related substances around the rebar in concrete and the assumed models for corrosion propagation, the amount of corrosive product and the possible time for the generation of the cracks due to corrosion may be qualitatively predictable. As for the prediction on the structural and durability performance in the acceleration and deterioration period, there exist few researches so far. On the other hand, to the authors' knowledge, although the assumed models used in those research works for describing the deterioration process in propagation period are rational, they are generally so simplified that the essence of the corrosion mechanism in concrete structures under corrosive environment during propagation period is neglected. This insufficiency caused those research works lack the ability to reflect the features of being-corroded steel (e.g. natural potential or polarization resistance, etc.), which have been often adopted in assessing the corrosion behavior of steel in concrete.

As a result, this research is motivated to supplement this insufficiency by proposing the electrochemical models, which can properly describe the dynamic process of the corrosion mechanism of concrete structures under corrosive environment. In this paper, one comprehensive numerical system for meeting the mentioned tasks is proposed. This numerical system is first explained in accordance with its constituent models related to the transport of corrosion-related substances such as chloride, oxygen and moisture

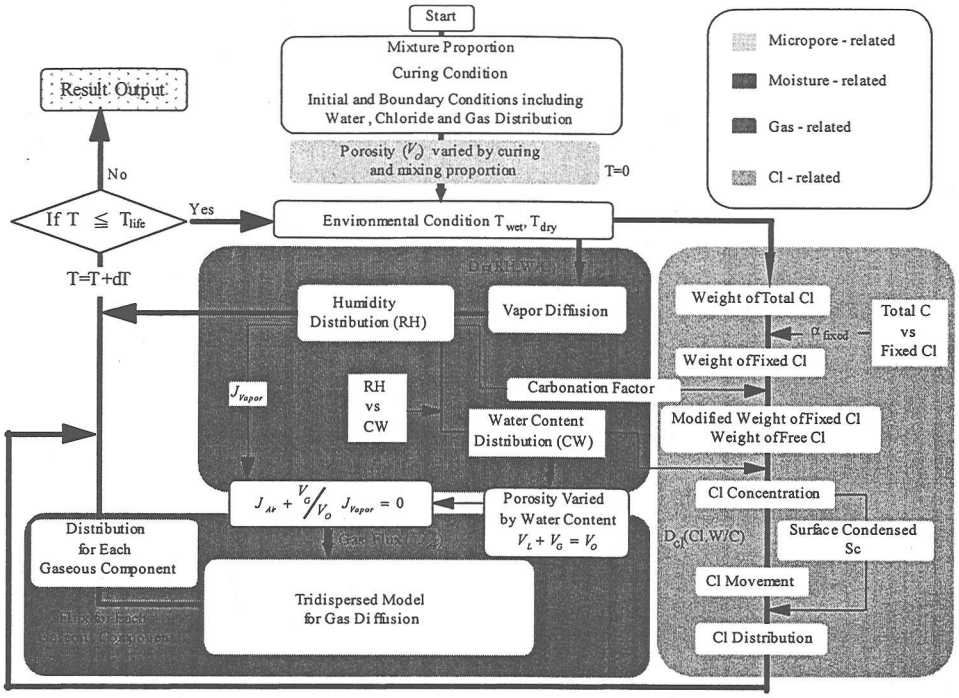

Fig.1 Computational flow for simulation on transport of corrosion-related substances in concrete

respectively. Then, the electrochemical models for simulating the formation of natural potential and corrosion current density are further clarified. Finally, experimental verification was executed to verify if this system on modeling the corrosion of steel in concrete structures under chloride attack is available or not. Besides, some discussions on the parameters considered in this numerical system are given for clarifying their influences in this numerical system.

2. DESCRIPTION ON COMPUTATIONAL MODELS

(1) Models for transport of corrosion-related substances

It is well known that the initiation of the corrosion of steel in concrete is strongly related to the soundness of the passive film around steel surface. If this passive film is destroyed, the corrosion process of steel in concrete is commonly believed to initiate, i.e. the termination of incubation period. The substances related to the destruction of the passive films in concrete are generally regarded as chloride ion, moisture, oxygen and carbon dioxide, etc. By integrating the past researches of the authors with the works of other researchers on the simulation for the transport of corrosion-related substances in concrete, one numerical system has been constructed by the authors[3], the computational flow of which is illustrated in **Fig.1**.

With the given mixture proportion, curing and environmental conditions, the model proposed by Shimomura and Maekawa[4] is adopted for tracing the real-time relationship between pore structure and moisture. As for simulating the moisture migration in concrete, the work of Saeki[5] *et al.* is utilized. Furthermore, by coupling the model relating to micropore structure with the model relating to the moisture migration in concrete, the real-time porosity at wet state (V_G, cm³/cm³) and the volume of liquid-phase water per unit volume (V_L, cm³/cm³) can be traced by vapor migration simulation.

Then, for simulating the migration of gaseous components in concrete, one model proposed by Hsu[6] *et al.* is adopted, the feature of which is to utilize the usual concept of equimolal counter diffusion for a constant pressure system. By applying this concept, their model assumes the inward flux of air (J_{Air},cm³/(cm²-day)) in the free space of pore should be equal to the outward flux of vapor (J_{Vapor}, cm³/(cm²-day)) in the free space of pore. In addition, under the consideration for the vapor gain due to evaporation and loss due to condensation, which is implicitly included in the

calculated outflux of vapor according to the empirical model[5] used for simulation of vapor migration in concrete, the expression of their model is suggested as follows:

$$J_{Air} + {}^{V_G}\!/_{V_O} \cdot J_{Vapor} = 0 \qquad (1)$$

Generally speaking, the concept of porosity and tortuosity should be introduced into the models for gas (or vapor) diffusion through porous solids, e.g. the micromechanical model established by Shimomura and Maekawa[4]. As for this aspect, in Eq.(1) , the concept of tortuosity is considered to be implicitly included in the calculation of the empirical model of the vapor migration while the concept of porosity is reflected in the simulation of the real-time pore structure as stated in the preceding models. Also, until present, through many investigations, the complexity of chloride diffusion in concrete is gradually recognized, resulting in the difficulty to find out the chloride distribution merely by applying the diffusion theory. The factors giving rise to the complexity are generally verified as the equilibrium between free and fixed chloride, the effect of carbonation, the effect of cyclic wetting and drying as well as the condensation effect in the surface layer. Among those existing models, the mathematical model proposed by Maruya[7] *et al.* is adopted because their model is successful in integrating all the above-mentioned factors. However, for the work of Maruya[7] *et al.* gives no consideration on the relationship between porosity, temperature and diffusivity of chloride, the work of Saetta[8] *et al.* is referred. Through the above models, the real-time transport and accumulation of corrosion-related substances in concrete can be simulated throughout the service life (T_{life}) of the structures. In addition, the environmental condition in **Fig.1** is referred to T_{wet} (the duration of the cyclic wetting) and T_{dry} (the duration of the cyclic drying).

(2) Models for corrosion of steel in concrete

As known, once the corrosion due to chloride attack initiates, the performance of structures will start to decrease. The degradation degree of performance depends on the corrosion rate. Before the generation of the corrosion cracks, the degradation degree of performance is comparatively small while, after the corrosion cracks generates, the degradation degree of performance becomes significantly large. In view of electrochemistry on corrosion, the degradation degree of performance is closely related to corrosion rate, which is in the form of current density. There are usually 3 types of approaches[9] on the state-of-the-art of the researches for modeling on the corrosion rate in concrete, which include 1) the models in the form of empirical relations; 2) the models related to the diffusion-limited process of oxygen and 3) the models based on the electrochemistry. Compared to the models belonging to approach 1 or 2, the models belonging to approach 3 are comparatively complicated. However, it seems that the models belonging to approach 3 take researchers' more interest. The reason can resort to the fact that not only the corrosion rate of steel but also the other features of being-corroded steel, such as natural potential or polarization resistance can be rationally simulated in these models. As known, natural potential (or polarization resistance) has been practically adopted in assessing the corrosion behavior of steel in concrete on lots of onsite measurement. Hence, based on the understanding for the electrochemical processes of corrosion, the models aiming at modeling on not only the corrosion rate of steel but on the natural potential are proposed by the authors[10], the characteristics of which are briefly explained as follows:

a) Kinetics of rebar corrosion reactions

For facilitating the following interpretation, a brief description on kinetics of corrosion reactions is given. As known, the high alkalinity of concrete ($pH \geq 12$) protects the steel from corrosion due to the formation of passive film. However, due to low alkalinity and/or high chloride content at the surface of the steel, the passive film breaks down. Owing to the difference in potential between anode and cathode, iron is oxidized to ferrous ions at the anode and oxygen is consumed due to the release of hydroxyl ions at cathode, half reactions of which are given below:

Anodic reaction (metal dissolution as Fe^{2+} ions)

$$Fe \Rightarrow Fe^{++} + 2e^- \qquad (2.a)$$

Cathodic reaction (oxygen reduction)

$$1/2O_2 + H_2O + 2e^- \Rightarrow 2OH^- \qquad (2.b)$$

By assuming the polarization of each half-cell reaction as the simplified adaptation of Butler-Volmer kinetics, the relationship between potential and current density can be expressed as:

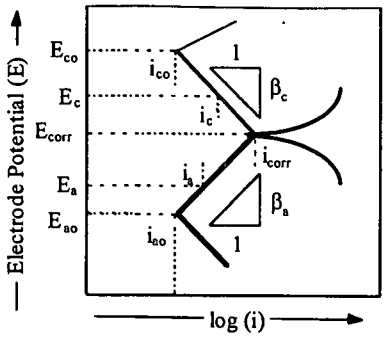

Fig.2 Polarization model on corrosion

$$\text{Anode} \quad : \quad E_a = E_{ao} + \beta_a \log(i_a/i_{ao}) \qquad (3.a)$$

$$\text{Cathode} \quad : \quad E_c = E_{co} + \beta_c \log(i_c/i_{co}) \qquad (3.b)$$

where a and c : anode and cathode; E : potential; E_{xo} : equilibrium potential at x (i.e. a or c); β_x : activation Tafel slope for x; i_x: current density for x; i_{xo}: exchange current density for x. As **Fig.2** shows, the equilibrium potential for anode and cathode reactions is termed as corrosion potential (E_{corr}) and the correspondent current density at this potential is called corrosion current density (i_{corr}). Customarily, the measured corrosion potential of steel in concrete is often termed as natural potential because it can be also considered as the being-interacted state of the steel under natural environment.

b) Pitting potential

As commonly observed, chloride corrosion in concrete usually takes place in the form of pitting corrosion. Also, the drop of pitting potential in concrete is related to the fall of pH in concrete and/or the gain of concentration of chloride. According to the two-step initiation theory of pitting corrosion suggested by Okada[11], the pitting initiation potential (E_{pit}) can be considered as the function of pH and chloride concentration. Similar relation was reported in the empirical work of Bird[12] *et al.* as follows:

$$E_{pit} = -0.015 - 0.31 \log([Cl^-]/[OH^-]) \qquad \text{(Vs. SCE)} \qquad (4)$$

where $[OH^-]$: hydroxyl ion (M) and $[Cl^-]$: free Cl^- ion (M). Indeed, besides the influence of pH and chloride concentration, it is commonly understood that many factors, such as the pore structure or water content of concrete, etc., also affect pitting potential; however, for the simplicity of this numerical system, only the effects of pH and chloride concentration are considered and the variation on pH in concrete is assumed to be the constant value during the simulation.

c) Chloride threshold value

In order to destroy the passive film, it is thought that there exists at least a certain amount of chloride leading to pit initiation followed by the occurrence of perturbation, accumulation of chloride ion at the local anodic sites and the nucleus formation at the passive film surface. As for the details for these processes, it can be referred to the "two-step initiation theory" suggested by the work of Okada[11]. This amount of chloride is usually termed as chloride threshold value. So far, the exact expression of chloride threshold value is still under argument, the reasons of which may result from many factors, such as the difficulty to clearly understand the real-time state of rebar surface or the adhesive state along the interface between rebar and concrete, etc. Nevertheless, by considering the integrity and the simplicity of this numerical system, a simple expression in the terms of threshold Cl^-:OH^- ratio is presently adopted by neglecting the above effects. The adopted expression is given by the regression analysis on the results of the limited experiments carried by the authors, the details of which are given in section 3 (Verification) of this paper. During the verification experiments, the minimum of total chloride amount was found out and converted to the free chloride ion according to the work of Maruya[7] *et al.* Because it is impossible to measure the value of pH during the experiments, the constant value of pH in concrete is assumed, which is the same as the value used in Eq.(4).Then, the threshold Cl^-:OH^- ratio is decided , which is shown as follows.

$$[Cl^-]/[OH^-] = 4.7 \qquad (5)$$

Within the review work of Glass and Buenfeld[13], it is mentioned that the threshold Cl^-:OH^- ratios determined in the pore solution expressed from concrete, mortar and cement paste specimens have varied more widely. For example, Yonezawa[14] *et al.* showed that the threshold Cl^-:OH^- ratios might be ranged from 1 to 40. Lambert[15] *et al.* reported that the ratios between 3 and 20 were required to initiate the corrosion of rebar in concrete. As a result, from the above comparison, the threshold Cl^-:OH^- ratio used in Eq.(5) is believed to be within acceptable scope. It is noteworthy that the value used in Eq.(5) is only used for numerical reference rather than the practical reference on judging the start of corrosion because of its over-simplicity.

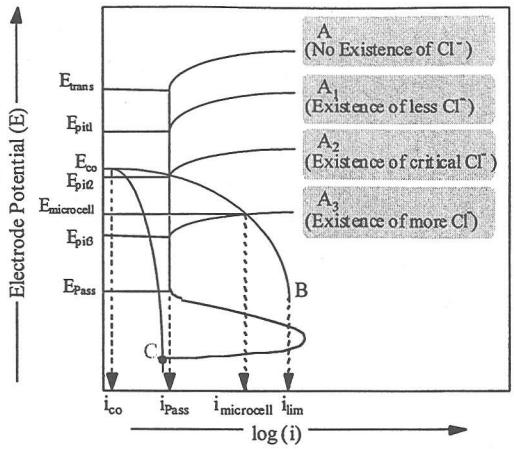

Fig.3 Model for microcell potential

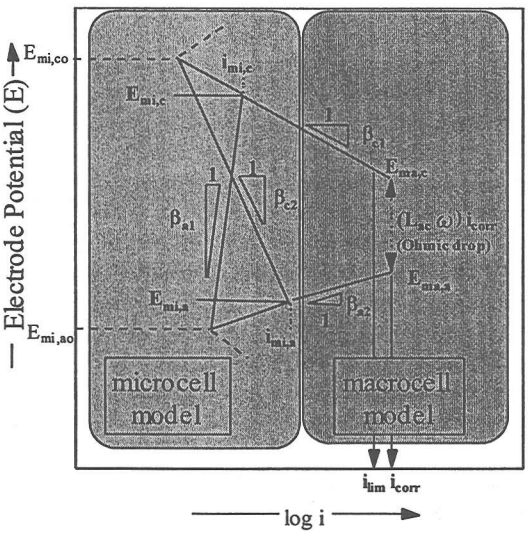

Fig.4 Model for macrocell current density

d) Model for microcell potential

The term "microcell" here is adopted for the assumption that the formation of the polarized potential at separate electrode (i.e. the point at the surface of rebar) is independent without the interaction between separate electrodes. If no pitting corrosion, the microcell potential can be regarded as the measured natural potential at its passive state. By observing the anodic and cathodic polarization curves as schematized in **Fig.3**, curve A depicts the case of no existence of Cl^-, under sufficient access of oxygen. The intersection (i.e. $E_{microcell}$, microcell potential) of curves A (or A_1, A_2 and A_3) and B must be located between E_{trans} (transpassive potential) and E_{pass} (passive potential). With the increase of Cl^-, the correspondent E_{pit} gradually drops. However, before reaching the threshold value of Cl^- (curve A_1), there is little influence from the drop of E_{pit} on the formation of $E_{microcell}$. In addition, once the chloride threshold value is exceeded (curve A_3), $E_{microcell}$ will be much lower than the correspondent E_{pit}. In other words, if E_{pit} is lower than the cathodic potential (E_c) at passive current density (i_{pass}), the pitting corrosion is initiated. Based on these understandings, the decision of $E_{microcell}$ can be achieved by comparing the relative location of E_c and E_{pit}. This comparison can lead to the judge of the initiation of pitting corrosion. In addition, if Nernst Equation is applied for anodic reaction, the correspondent microcell current density ($i_{microcell}$) can be calculated.

e) Activation polarization

In the previous section, under the assumption that there exists no interaction between separate electrodes, the algorithm to calculate $E_{microcell}$ of rebar under chloride corrosion is illustrated. However, once pitting corrosion is initiated, there should be the interaction between separate electrodes due to the existence of polarization. As a result, the model for macrocell corrosion is established by assuming the formation of macrocell as the interaction between separate electrodes. According to the assumption used in the previous section, after the formation of microcell potential, the state of separate electrodes should be regarded as stable due to no interaction between separate electrodes. However, once the interaction between separate electrodes is taken into account, the activation polarization is indispensable for generating the essential activation energy needed in the corrosion reactions. As illustrated in **Fig.4**, for any two electrodes, if pitting corrosion is initiated, the macrocell current density (i_{corr} , unit: A/cm²) can be calculated by solving the following nonlinear equation:

$$\begin{aligned} & E_{ma,c} - E_{ma,a} \\ & = (L_{ac}\omega)\, i_{corr} \\ & = (E_{mi,c} + \beta_{c1} \log(i_{corr}/i_{mi,c})) - \\ & \quad (E_{mi,a} + \beta_{a2} \log(i_{corr}/i_{mi,a})) \end{aligned} \tag{6}$$

where *ma* : macrocell; *mi* : microcell; L_{ac} : distance between anode and cathode (cm); ω: concrete resistivity (Ω-cm). For Tafel slope (i.e. β_{a2} and β_{c1}), the empirical expressions reported by Japan Concrete Institute (JCI) committee on repair methods of concrete structures[16] are adopted for the compatibility on RC structures, which are shown as follows.

$$\beta_{a2} = -0.012139\, ln(Cl^-) + 0.1916 \quad \text{(V/decade)} \quad (6.a)$$

$$\beta_{c1} = -0.037379\, ln(Cl^-) + 0.2597 \quad \text{(V/decade)} \quad (6.b)$$

where Cl^- : concentration of free chloride per unit volume (lb/m^3). Generally, it is thought that not only the concentration of chloride ion but also the mixing proportion (e.g. the type of cement) and the environment around the rebar (e.g. the water content), etc. influence the Tafel slope (i.e. β_{a2} and β_{c1}). The proper empirical expression for Tafel slope should take the above effects into consideration; however, in the literature, there seems to be still no such finding to consider the effects of all these factors. Once it is available, the empirical expressions given in Eq.(6.a) and (6.b) ,which merely consider the effect of concentration of chloride ion, should be correspondently modified. In addition, in order to solve the above nonlinear equation Eq.(6), the method of false position is utilized.

Once i_{corr} is solved so that, for anode, the value of i_{corr} takes negative to indicate the inflow of electronic current while, for cathode, that of i_{corr} takes positive to indicate the outflow of electronic current.

f) Limiting current density

Due to the cover thickness of concrete, saturation degree of concrete and environmental conditions, etc., the access of O_2 at the surface of passive film may be insufficient, which renders corrosion reaction diffusion-limited. Furthermore, if this insufficiency of access of O_2 is severe, the formatted potential may be even lower than E_{pass}, which can be referred to point C in **Fig.3**. This phenomenon is often observed for the RC structures submerged under the sea. In this paper, the limiting current density of O_2 (i_{lim}, A/cm^2) suggested by JCI[16] is adopted as follows.

$$i_{lim} = \frac{M}{2.591 \times 10^{-6}} \quad (7)$$

where M: the supply flux of O_2 at the surface of rebar in concrete ($mol/(s\text{-}cm^2)$).

g) Model for macrocell current density

As have been explained, the model schematized in **Fig.4** is valid for any two electrodes once pitting corrosion is initiated. However, as known, there are usually lots of electrodes distributed along any rebar. That is to say, for any electrode, there should exist multiple electrical circuits. To obtain the net current density within the multiple electrical circuits, the following steps are taken:

Step 1. For N electrodes along the rebar, the number of the possible electrical circuits is 1/2N(N-1). By applying Eq.(6) for all the possible electrical circuits, the anodic and cathodic current density for each circuit can be obtained. In other words, there is no need to specify the location of anode and cathode (or the area ratio of anode with respect to cathode) before the calculation, i.e. they will be specified automatically due to the service situation of the exposure environment.

Step 2. By taking the integration of macrocell current density (i_{corr}) at each electrode along the rebar, the net macrocell current density at each electrode can be calculated as follows.

$$i_{corr,net} = \int_0^L i_{corr}\, dx \quad (8)$$

where $i_{corr,net}$: net macrocell current density, unit: A/cm; L : length of the rebar

Step 3. By the sign convention of $i_{corr,net}$, the correspondent electrode can be judged as anode (if sign < 0) or cathode (if sign > 0).

Through the above steps, $i_{corr,net}$ at each electrode can be available. Then, the following equation is utilized for converting the calculated $i_{corr,net}$ (A/cm) to the corroded amount of Fe[16]:

$$W\{Fe\} = (3987.594/r) \cdot i_{corr,net} \quad (9)$$

where $W\{Fe\}$: the corroded amount of Fe ($mg/(cm^2\text{-}day)$); r : radius of the rebar (cm). Moreover, the corrosive depth of the rebar can be also calculated by following the below expression:

$$h\{Fe\} = (T \cdot W\{Fe\})/\rho \quad (10)$$

where $h\{Fe\}$: the corrosive depth of the rebar (cm); T : duration for corrosion occurrence (day) and ρ : the density of Fe (=7860 mg/cm^3).

h) Model for macrocell (natural) potential

As can be observed in **Fig.4**, the microcell potential at separate electrode is polarized due to the activation and/or concentration (i.e. diffusion-limited) polarization. Through the above model, due to the existence of multiple electric circuits, the possibility to own different amount of polarization for an electrode contradicts the reality of the measured natural potential of the rebar. As a result, there is the need to modify the calculated macrocell (natural potential). However, up to now, there is little research reported on how the process of the being-polarized rebar should be. The

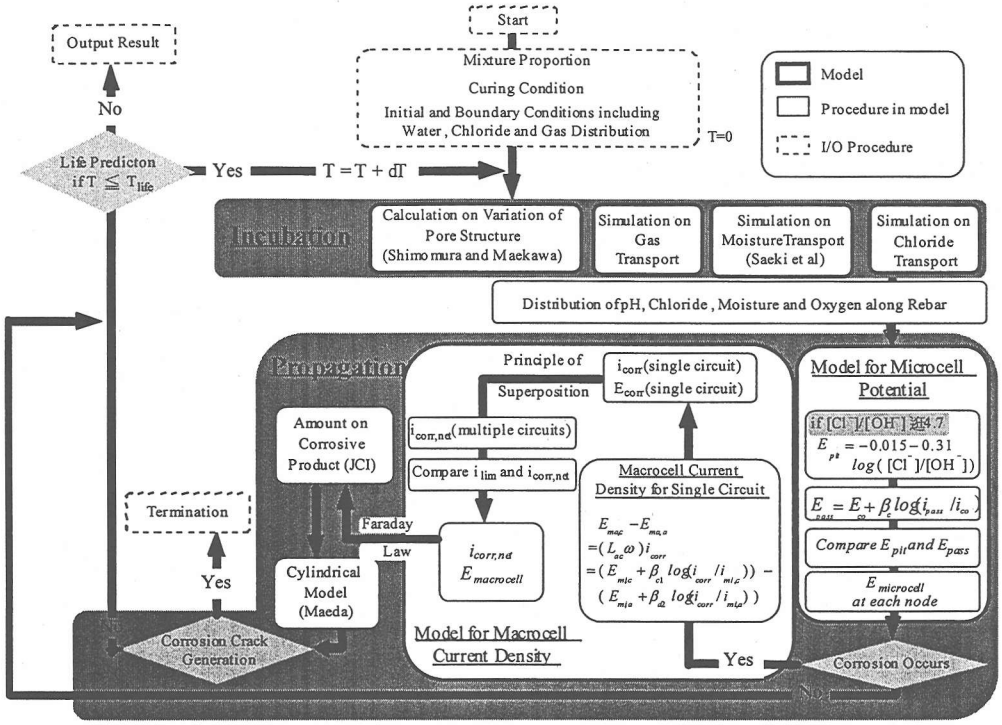

Fig.5 Computational flow for simulation in incubation and propagation period

modification on the calculated macrocell (natural potential) is implemented by taking the average amount of polarization for an electrode owing to its simplicity. Then, the distribution of macrocell (natural) potential along the rebar can be calculated.

i) Critical corrosive depth

In order to judge if the propagation period is terminated or not, the way to calculate critical corrosive depth Δx (cm) is usually acted as the criterion for the initiation of the corrosion crack. According to review report of JCI committee[17], there exist several proposals to calculate the critical corrosive depth, such like the proposal considered by Maeda[18], the proposal considering restrained displacement or the proposal considering volume expansion, etc. Within these proposals, the proposal considered by Maeda[18] (denoted Maeda's method) is based on the elastic theory. Due to the simplicity and the same prediction level of the result obtained by Maeda's method, Maeda's method is adopted in this paper. Once the corrosive depth in Eq.(10) exceeds the critical corrosive depth, the simulation process mentioned in this paper will be terminated for the simulation process in the existence of corrosion cracks is not the interest of this paper.

j) Integration on models for simulation

Followed by the explanations on the characteristics of the electrochemical model, **Fig.5** illustrates the integration of the aforementioned features of the proposed models in propagation period, in which the details on the models in incubation period as illustrated in **Fig.1** are skipped. Moreover, in **Fig.5**, in order to distinguish the models proposed by the past works of the authors from the models proposed by other researchers or institutes, the models followed by the name(s) in parenthesis indicate they are the ones proposed by other researchers or institutes.

3. VERIFICATIONS

(1) General

In order to verify the aforementioned numerical system, some indoor experiments were used for the comparison with the simulated results according to the numerical system described in the preceding section. These experiments were implemented under various experimental conditions. The material parameters used for this numerical system were adopted from the assumption of its constituent models based on the given mixture proportion and

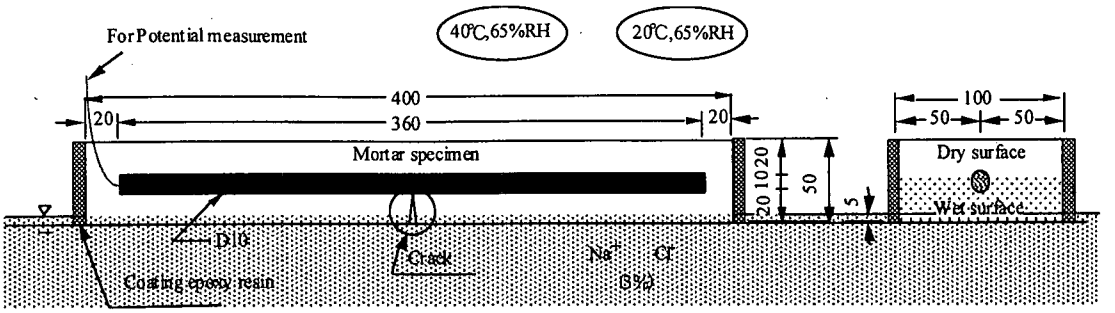

Fig.6 Layout and setup of the specimen in indoor experiment

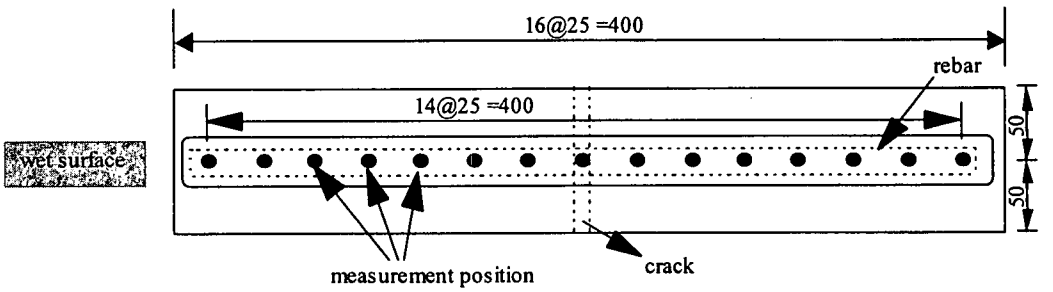

Fig.7 Illustration of measurement position for corrosion potential

Table 1 Type and required specification for material

Material	Type	Specification
Rebar	SD295,D10	JIS G 3112
Cement	Portland cement	JIS R 5210
Admixtures	AE water reducing agent	JIS A 6206
Fine aggregates	Pit sand	JSCE concrete code (construction part)[19]
Coarse aggregates	Crashed limestone	
Water	Tap water	—

Table 2 Mixture proportion of mortar

W/C	S/C	Unit weight (kg/m³)			
(%)	(%)	W	C	S	AE water reducing agent
40	1.83	262	655	1201	C x 0.25wt%
50	2.50	262	526	1308	C x 0.25wt%

environmental condition. The availability of this numerical system was discussed through comparing the computed results of the corrosion-related substances and the electrochemical characteristics with experimental ones.

(2) Outline of the experiments

18 reinforced mortar specimens (400 mm wide, 100 mm deep and 50 mm high with concrete cover thickness = 20mm) were exposed under various conditions for 22 weeks. The indoor experiments were carried out by simulating the site with high chloride concentration groundwater from the bottom surface and intense evaporation of water into the air from the top surface, the layout and setup of which are illustrated in **Fig.6**. As indicated in **Fig.6**, the bottom part of the specimen up to 5mm depth was immersed into the simulated groundwater and the chloride ion concentration in simulated groundwater was made nearly as 3% of NaCl solution. Besides, to limit the movement of chloride only in the vertical direction, all the side surfaces of each specimen were coated by epoxy resin. The experimental conditions were varied in accordance with:

- water-cement ratio by weight: 40% and 50%
- exposure-temperature: 20°C and 40°C
- cracked specimens and uncracked specimens

As a result, there are totally 6 experimental conditions, the results for each of which were taken from the average of every 3 specimens. As for the type and the required specifications for rebar, cement, admixtures and aggregates, they are given in **Table 1**. The mixture proportions of mortar are shown in **Table 2**. The various experimental conditions are shown in **Table 3**. The slump flow value and air content were measured between 229~256 mm and 5.5~7.0% respectively. The crack in each cracked specimen was introduced in central zone at the bottom of each specimen by conducting

tests of three-point bending. Furthermore, the method to measure the corrosion potential can be referred to the report of JCI committee on repair methods of concrete structures[20]. The location of measurement on specimen was implemented at wet surface, the measurement positions of which are illustrated in **Fig.7**. As for the method to measure the distribution of the total chloride amount, it follows standard steps of the suggested method JCI-SC5 by JCI[21]. **Fig.8** shows the samplings for measuring the distribution of total chloride amount in cracked and uncracked specimens.

(3) Computational method

The previously described models for simulation in incubation and propagation period result in a system of partial differential equations governing the corrosion process. A closed-form solution of this system of equations is impossible due to the interdependence of the models one another. However, this system of equations can be solved numerically in space as a boundary value problem and in time as an initial value problem by means of two-dimensional finite element (FE) formulation, the FE formulation of which can be referred to the work of Balabanic[22] et al. The numerical solutions for this system of equations are achieved by using Crank-Nicholson method.

a) Chloride transport through crack surface

As for the chloride transport through the crack surface in the specimens, the following assumptions were made. First, set the relationship for the flux (S_{crack}) through the crack surface to the flux (S_{sound}) through the sound surface as follows.

$$SS = S_{crack}/S_{sound} \tag{11}$$

where SS : the ratio between S_{crack} and S_{sound}, the value of which is greater than 1.0. Then, define the ratio for the surface area at the crack surface to the surface area at the sound surface as κ. The value of κ is also greater than 1.0. Here, it can be understood that the definition of SS and κ is both dependent on the existence of cracks. Therefore, it can be assumed that the crack surface has the same influence level on the increased degree of the flux through the crack surface and the surface area at the crack surface, i.e. assuming $SS = \kappa$. Because of this assumption, S_{crack} can be taken as $S_{crack} = \kappa \cdot S_{sound}$. Generally speaking, the prevailing approach for the chloride transport through the crack surface is achieved by setting the diffusion coefficient at the crack surface as several times of the diffusion coefficient at the sound surface (e.g., the work of Ishida[23] *et al.*), which lacks the substantial support on the physical process. On the contrary, although there exists the difficulty on clarifying the definite value of SS and κ, the reasonableness of the proposed assumptions appear to be supported by the assumed physical process. As a result, the above model is introduced in calculating chloride transport through the crack surface. As for the value of κ, it is assumed by fitting the calculated total chloride amount at the crack surface to the experimental results, which is ranged from 1.5 to 5.0.

Table 3 Case for various experimental conditions

Case label	1M	2M	3M	4M	5M	6M
W/C (%)	40	40	50	50	50	50
S/C (%)	1.83	1.83	2.50	2.50	2.50	2.50
Cracked specimen	yes	no	yes	yes	no	no
Width of crack (mm)	0.06	0.0	0.07	0.07	0.0	0.0
Temperature (°C)	40	40	40	20	40	20
Humidity (%RH)	65	65	65	65	65	65

Table 4 Material parameters for simulation

Parameters \ Case			1M	2M	3M	4M	5M	6M
Diffusion coefficient (10^{-3} cm²/day)	Water	surface	83.6	83.6	145	66.2	145	66.2
		inner	22.6	22.6	46.0	18.1	46.0	18.1
	Chloride	surface	4.24	4.24	7.16	2.04	7.16	2.04
		inner	3.53	3.53	5.97	1.70	5.97	1.70
Resistivity (ω) (10^4 Ω-cm)			2.70	2.70	2.90	7.40	2.90	7.40
Surface increased ratio (κ)	Sound	surface	1.0	1.0	1.0	1.0	1.0	1.0
	Cracked	surface	1.5	0.0	1.5	1.5	0.0	0.0

b) decision of parameters for simulation

The essential parameters used for each case in the simulation are listed in **Table 4**. The calculation on the resistivity for the mortar specimen was referred to the work of Saeki[24] *et al.* In the paper of Saeki *et al.*, they experimentally found that the resistivity of mortar depends on the degree of hydration and carbonation, the water content of mortar and temperature. As a result, in their work, the resistivity of the mortar is defined as the multiplication function of the above factors.

4. RESULTS AND DISCUSSION

(1) State corrosion of rebars

In order to understand if the rebars in the specimens is corroding or not, the specimens were split at 10th, 16th and 22nd week to check the corrosion state of the rebars by eye-measurement, the results of which are shown in **Table 5**. From **Table 5**, the following observations on the state

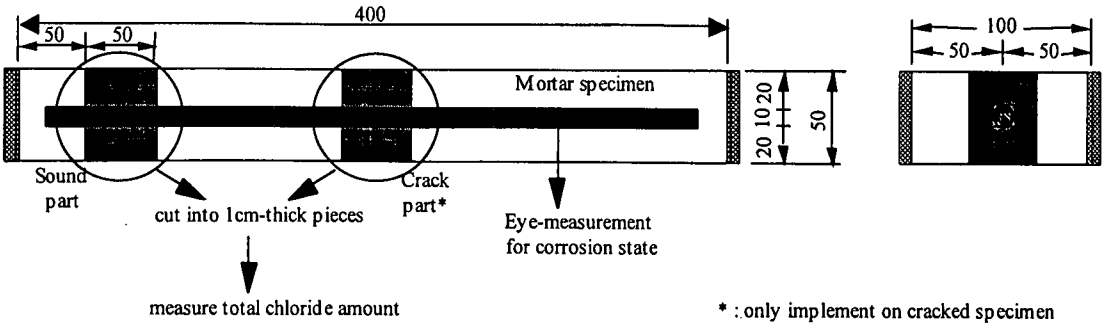

Fig.8 Illustration of samplings from specimen for measuring total chloride amount

corrosion of rebars can be obtained. First, regardless of the type of mixture proportion and the exposure environment, the lower surface (i.e. the surface near the wet surface) of the rebars in all the cracked specimens were found to be corroding after 10 weeks exposure. In addition, the upper surface (i.e. the surface near the dry surface) of the rebars in all the cracked specimens except for case 4M was also found to be corroding after 10 weeks exposure. Secondly, for the uncracked specimens, case 5M was found to be corroding after 10 weeks exposure while case 2M and 6M were found to be corroding after 22 weeks exposure. On the other side, the simulated results on the variation of the maximum ratio of $[Cl^-]$ and $[OH^-]$ along rebar with respect to time for each case are shown in **Fig.9**. **Fig.9** indicates the agreement for judging the start period of corrosion with experimental observation results in each case by introducing the chloride threshold value given in Eq.(5).

Table 5 Corrosion check on rebar by eye-measurement

Observation \ Case		1M	2M	3M	4M	5M	6M
Corroded at 10th week	upper surface	yes	no	yes	no	no	no
	lower surface	yes	no	yes	yes	yes	no
Corroded at 16th week	upper surface	yes	no	yes	yes	yes	no
	lower surface	yes	no	yes	yes	yes	no
Corroded at 22nd week	upper surface	yes	no	yes	yes	yes	yes
	lower surface	yes	yes	yes	yes	yes	yes

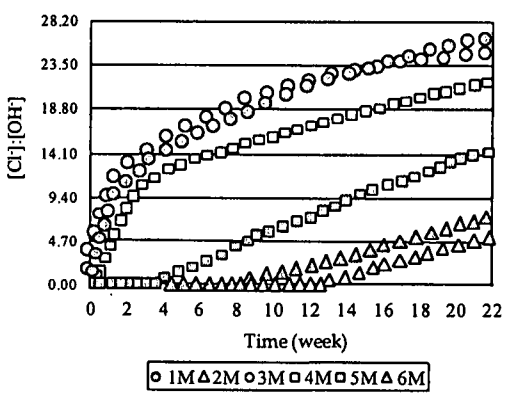

Fig.9 Maximum $[Cl^-]:[OH^-]$ along rebar with respect to time

(2) Penetration of chloride ion

As for the penetration of chloride ion, the experimental results for the distribution of total chloride amount in cracked and uncracked specimens at 22nd week are reported in **Fig.10** and **Fig.11** respectively, the cases of which are labeled as EXP. It is clearly found that the upward movement of chloride ion in cracked specimens is more significant than in uncracked specimen. In addition, based on the parameters given in **Table 3** and the algorithms for calculating the transport of corrosion-related substances, the simulated results for the distribution of total chloride amount on for the distribution of total chloride amount on cracked specimens 1M,3M and 4M are shown in **Fig.10(a),(b)** and **(c)** while, for uncracked specimens 2M,5M and 6M, their results are given in **Fig.11(a),(b)** and **(c)**. From these comparisons, the agreement between experimental and simulated results verifies the availability of the numerical system on predicting the transport of corrosion-related substances in concrete.

(3) Corrosion potential

As for the distribution of corrosion potential of the specimens, the experimental results on cracked specimens are shown in **Fig.12(a)-(c)** individually. It can be easily observed that the value of corrosion potential near the crack preexisted in the specimen

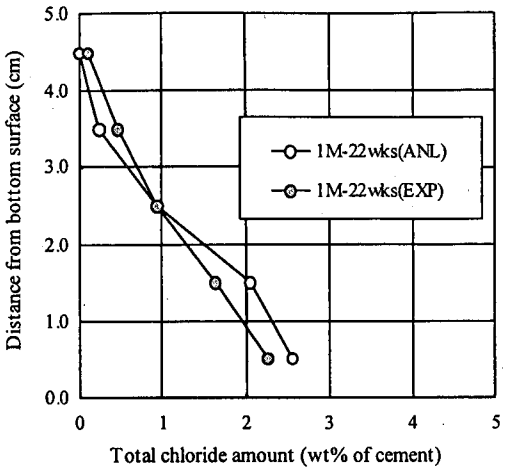

Fig.10(a) Total chloride content in cracked specimen (1M)

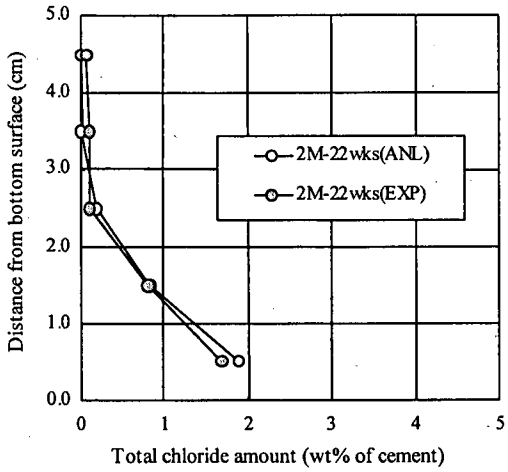

Fig.11(a) Total chloride content in uncracked specimen(2M)

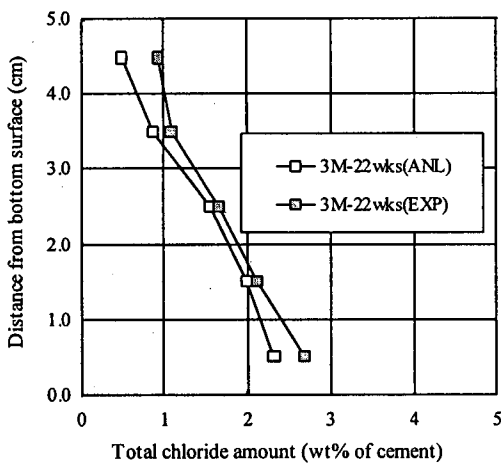

Fig.10(b) Total chloride content in cracked specimen (3M)

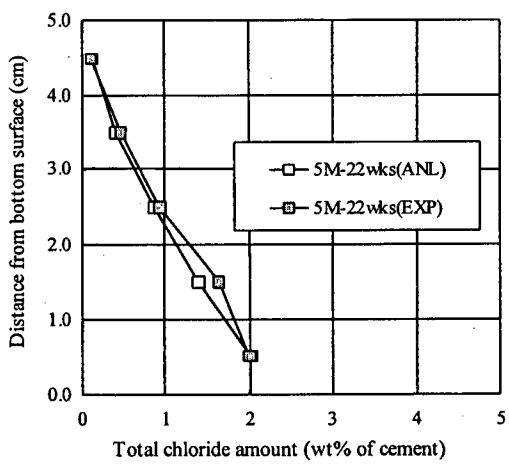

Fig.11(b) Total chloride content in uncracked specimen (5M)

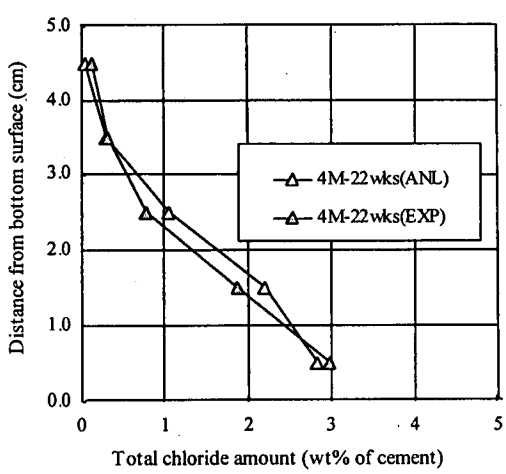

Fig.10(c) Total chloride content in cracked specimen (4M)

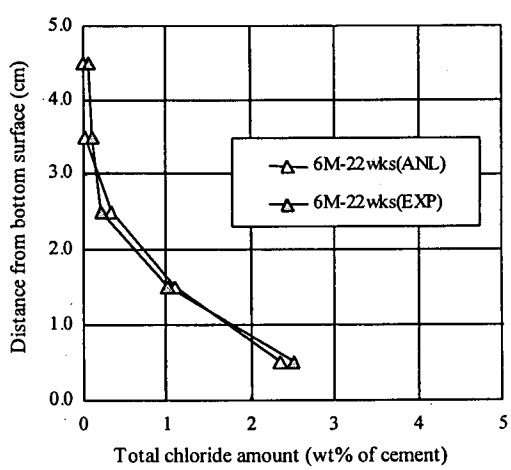

Fig.11(c) Total chloride content in uncracked specimen (6M)

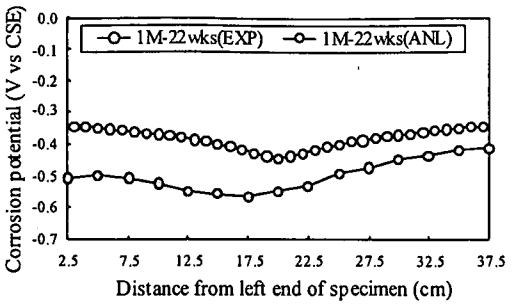

Fig.12(a) Corrosion potential distribution in cracked specimen (at wet surface) (1M)

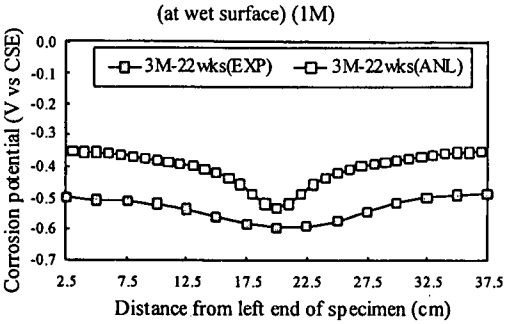

Fig.12(b) Corrosion potential distribution in cracked specimen (at wet surface) (3M)

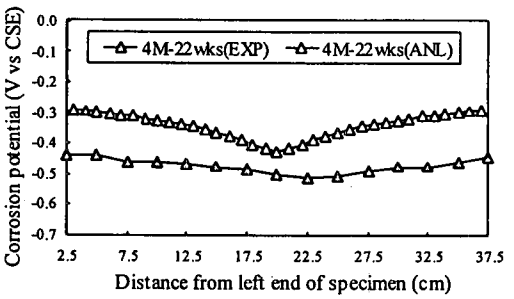

Fig.12(c) Corrosion potential distribution in cracked specimen (at wet surface) (4M)

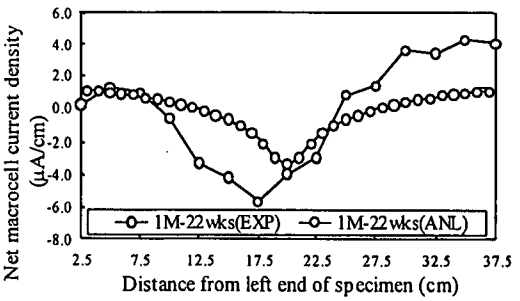

Fig.13(a) Macrocell current density in uncracked specimen (converted from corrosion potential) (1M)

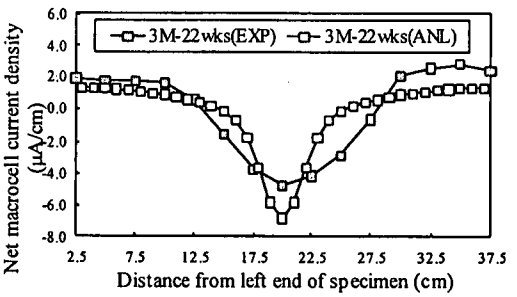

Fig. 13(b) Macrocell current density in uncracked specimen (converted from corrosion potential) (3M)

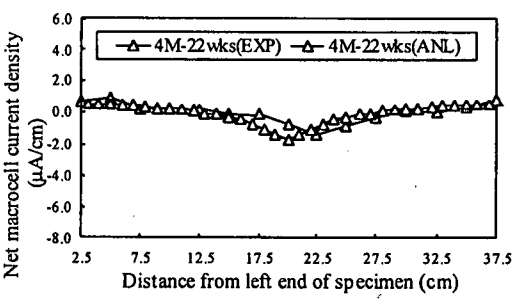

Fig.13(c) Macrocell current density in uncracked specimen (converted from corrosion potential) (4M)

is lower than that of corrosion potential at the parts without cracks, the reason of which can be related to the initiation of the corrosion of the rebar at crack. Besides, based on the electrochemical models including microcell and macrocell models as well as FEM formulation of Laplace equation, the simulated results for the distribution of corrosion potential at wet surface on cracked specimens are also shown in **Fig.12(a)-(c)** respectively. By comparing the experimental and simulated results in **Fig.12(a)-(c)**, the deviation may be resorted to the ambiguity on describing the quantitative relationship between the electrochemical characteristics (e.g. the pitting potential of steel in concrete, the Tafel slope and the resistivity) and the corrosion-related substances including chloride, moisture and oxygen. If the precise relationship between them can be well described, it is believed that the deviation between experimental and simulated results can be diminished.

(4) Macrocell current density

Based on the measured (or simulated) corrosion potential, the net macrocell current density can be converted. The results for both of them on cracked specimens are given in **Fig.13(a)-(c)**, in which the positive value corresponds to cathode while the negative value correspond to anode. From **Fig.13(a)-(c)**, it can be inferred that there should be serious corrosion at the central section of the rebars in the cracked specimens because large negative value can be seen near the central section of the rebar due to the pre-existed cracks. According to the results of eye-measurement on the spilt specimens, the real domain under corrosion was found to be almost the same location inferred by the distribution

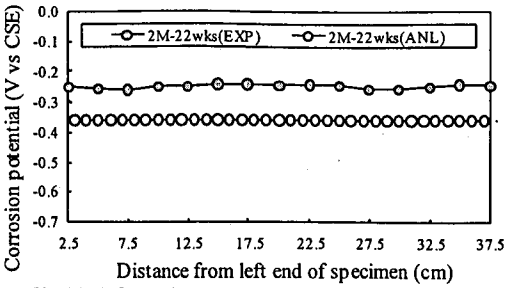

Fig.14(a) Corrosion potential distribution in uncracked specimen (at wet surface) (2M)

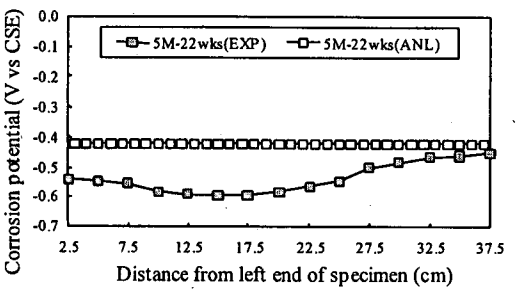

Fig.14(b) Corrosion potential distribution in uncracked specimen (at wet surface) (5M)

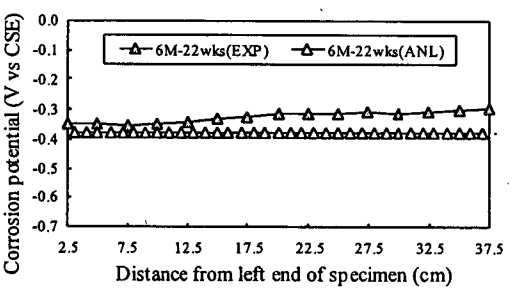

Fig.14(c) Corrosion potential distribution in uncracked specimen (at wet surface) (6M)

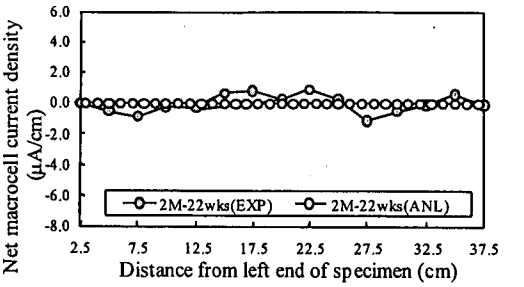

Fig.15(a) Macrocell current density in uncracked specimen (converted from corrosion potential) (2M)

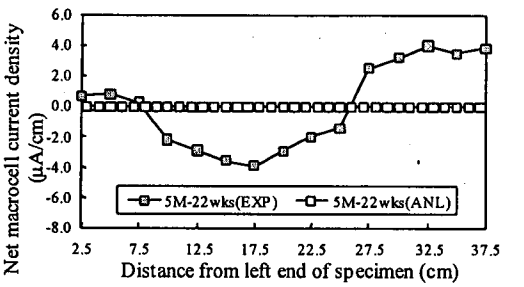

Fig.15(b) Macrocell current density in uncracked specimen (converted from corrosion potential) (5M)

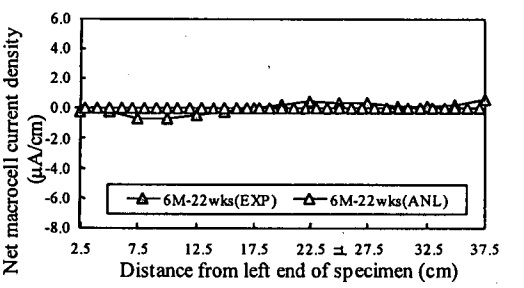

Fig.15(c) Macrocell current density in uncracked specimen (converted from corrosion potential) (6M)

of net macrocell current density. Through this discussion, it can be understood that the distribution of net macrocell current density is helpful for locating the domains under corrosion, i.e. the location of anode.

(5) Influence of crack

Through the previous discussions, it can be indicated the existence of pre-existed crack introduced by three-point bending test has significant influence on the corrosion state of the rebar by deriving the corrosion resistance around the crack and arousing early corrosion occurring at the rebar near the crack. By assuming proper model for the transport of corrosion-related substances through the crack and combing the proposed electrochemical models, the agreement between experimental and simulated results on the distribution of total chloride amount, corrosion potential and net macrocell current density can be observed in **Fig.10**, **Fig.12** and **Fig.13**. On the other hand, the correspondent comparisons for uncracked specimens are given in **Fig.11**, **Fig.14** and **Fig.15**. From these figures, the following observations can be found. First, as shown in **Fig.11**, with appropriate parameters for predicting the transport of corrosion-related substances, the prediction on the corrosion-related substances can be achieved. Also, the simulated value of the distribution of the corrosion potential of the uncracked specimens shows the start of the corrosion at 22nd week as shown in **Fig.14**. Nevertheless, as shown in **Fig.14**, there exists the deviation between experimental and simulated results. The reasons for this deviation may be resorted to not only the same one as mentioned for cracked specimens but the homogeneity of transgression of corrosion-related substances introduced in the process of simulation

for uncracked specimens. In fact, although there is no need for assuming the model for the transport of corrosion-related substances through the crack in uncracked specimens, the uncertainty of the location of anode(s) gives rise to the difficulty for simulating the net macrocell current. That is to say, for the process of simulation, the heterogeneity (i.e. the existence of cracks) of transgression of corrosion-related substance in cracked specimens makes it easy to specify the location of anode. On the other hand, the homogeneity (i.e. no existence of cracks) of transgression of corrosion-related in uncracked specimens make it difficult to specify the location of anode. As a result, as shown in **Fig.15**, the simulated results indicate there was no net macrocell current density while the experimental results point out there was the occurrence of corrosion for the cases of uncracked specimens after 22 weeks exposure. Moreover, the location of anode(s) for the occurrence of corrosion on uncracked specimens, which was observed in the experimental results, cannot be predicted in the simulated results.

5. CONCLUDING REMARKS

Through the algorithms explained and the experimental discussions in the preceding sections, the following conclusions can be extracted from this paper:

(1) The ability to trace time-dependent response of chloride-induced macrocell corrosion is recognized.
(2) However, there is the further need to verify the definitely quantitative relationship between the electrochemical characteristics and corrosion-related substances.
(3) In addition, for the process of simulation, the task for solving the uncertainty of the location of anode(s) derived from the homogeneity of transgression of corrosion-related substances also needs further investigation.

REFERENCES

1) Miyagawa, T., Masuda, Y., Takewaka, K., Moriwake, A., Ueda, T.: Proper application of rehabilitation methods for concrete structures deteriorated by chloride-induced corrosion, *Proc. 2nd Int'l RILEM/CSIRO/ACRA Conference on Rehabilitation of Structures*, pp.557-568, Sep. 1998.
2) Takewaka, K. , Hamada, H. and Ohta, T.: Deterioration Mechanism and Rehabilitation on Concrete Structures, *Concrete Journal, JCI*, Vol.36 No.7, pp.6-10, Jul. 1998. (in Japanese)
3) Maruya, T. and Hsu, K.L.: Numerical simulation on Cl^-, moisture, O_2 and CO_2 in concrete, *42nd Proc. of Japan Congress on Materials Research*, Sep. 1998. (in Japanese)
4) Shimomura, T. and Maekawa, K.: Analysis of the drying shrinkage behavior of concrete using a micromechanical model based on the micropore structure of concrete, *Mag. Conc. Res.*, Vol.49 No.181, pp.303-322, Dec. 1997.
5) Saeki, T., Ohga, H. and Nagataki, S.: Mechanism of carbonation and prediction of carbonation process of concrete, *Proc. of JSCE*, No.414/V-12, pp.99-108, Feb. 1990. (in Japanese)
6) Hsu, K.L. , Takeda, H. and Maruya, T.: Numerical simulation on migration of oxygen and carbon dioxide in concrete, *Proc. of JCI*, Vol.20 No.1, pp.769-774, 1998.
7) Maruya, T., Tangtermsirikul, S. and Matsuoka, Y.: Modeling of chloride ion movement at the surface layer of hardened concrete, *Proc. of JSCE*, No.585/V-38, pp.79-95, Feb. 1998. (in Japanese)
8) Saetta, A.V., Scotta, R.V. and Vitaliani, R.V. : Analysis of chloride diffusion into partially saturated concrete, *ACI Materials J.*, V-90, No.5, pp.441-451, 1993.
9) Japan Conc. Inst., Technical report on material design and performance of concrete structures, *Symposium on Material Design and Performance of Concrete Structures*, pp.162-180, May 1999. (in Japanese)
10) Hsu, K.L. and Maruya, T.: Modeling time-dependent response of chloride-Induced macrocell corrosion of steel in concrete, *Proc. of JCI*, Vol.21, No.2, pp.1009-1014, 1999.
11) Okada, T.: Two-step initiation theory of pitting corrosion in passive metals, *Boshoku Gijutsu*, Vol.36, pp.787-794, 1987.
12) Bird, H.E.H., Pearson, B.R. and Brook, P.A.: The breakdown of passive films on iron, *Corrosion Science*, Vol.28, No.1, pp.81-86, 1988.
13) Glass, G.K. and Buenfeld, N.R.: The presentation of the chloride threshold level for corrosion of steel in concrete, *Corrosion Science*, Vol.39, No.5, pp.1001-1013, 1997.
14) Yonezawa, T., Ashworth, V. and Procter, R.P.M.: The mechanism of fixing Cl- by cement resulting in the transformation of NaCl to NaOH, *Proc. 8th International Conference on Alkali-Aggregate Reaction*, pp.153-160, 1989.
15) Lambert, P., Page, C.L. and Vassie, P.R.W.: Investigations of reinforcement corrosion. 1. the pore electrolyte phase in chloride-contaminated concrete, *Material & Structures*, 24, pp.243-252, 1991.
16) Japan Conc. Inst., *Technical report on repair methods of concrete structure (III)*, pp.198-212, Oct. 1996. (in Japanese)
17) Japan Conc. Inst., *Technical report on repair methods of concrete structure (III)*, pp.226-232, Oct. 1996. (in Japanese)
18) Maeda, K.: Study on corrosion content of steel bar needed to cracking of concrete cover using electronical corrosion test, *Summaries Tech. Papers Ann. Meeting*

Archit. Inst. Japan, pp.147-148, Sep. 1983. (in Japanese)

19) Japan Society of Civil Engineers., *Standard specification for concrete structures [construction]*, 1996. (in Japanese)

20) Japan Conc. Inst., *Technical report on repair methods of concrete structure*, p.35, Oct. 1992. (in Japanese)

21) Japan Conc. Inst., *Test methods and specifications for corrosion and anticorrosion of concrete structures*, 1987. (in Japanese)

22) Balabanic, G., Bicanic, N. and Durekovic, A.: Mathematical modeling of electrochemical steel corrosion in concrete, *J. Eng. Mech.*, Vol.122, No.12, pp.1113-1122, Dec. 1996.

23) Ishida, T., Chaube, R.P., Kishi, T. and Maekawa, K.: An integrated computational system of mass/energy generation and transport, and material mechanical behavior, *Proc. of JCI*, Vol.20 No.2, pp.233-238, 1998. (in Japanese)

24) Saeki, T., Ohga, H. and Nagataki, S.: Quantitative estimation of steel corrosion in mortar due to carbonation, *Proc. of JSCE*, No.532/V-30, pp.55-66, Feb. 1996. (in Japanese)

(Received September 30 , 1999)

塩害によるコンクリート中の鋼材の腐食モデルに関する解析手法の構築

許鎧麟・武田均・丸屋剛

著者らは，腐食性環境下に置かれた鉄筋コンクリート構造物の性能の経時変化を予測することを目的として，既往の研究および著者らのこれまでの研究成果をもとに，鉄筋コンクリート構造物の細孔組織構造の形成，塩分，酸素と水分の移動過程，自然電位の形成および腐食電流密度を個々の現象に立脚したモデルを用いて連成解析する手法を構築した．本論文では，実験結果と解析結果を比較することにより，任意の配合，使用材料，材齢，養生条件，環境条件に対し，鉄筋コンクリート部材中の腐食因子の移動，蓄積及び鉄筋の腐食進行を適切に計算できることを明らかにした．